Engineering Fracture Mechanics Vol. 46, No. 3, pp. 413–432, 1993
Printed in Great Britain.

0013-7944/93 $6.00 + 0.00

ANALYSIS OF DEFORMATIONS NEAR A CRACK TIP IN A COMPRESSIBLE NONLINEAR ELASTIC MATERIAL

R. C. BATRA and J. P. ZHANG

Department of Mechanical and Aerospace Engineering and Engineering Mechanics, University of Missouri-Rolla, Rolla, MO 65401-0249, U.S.A.

Abstract—Finite plane strain deformations of a compressible nonlinear elastic body made of a Blatz–Ko material and containing an elliptical void are studied. The void is assumed to be either in the interior of the infinite body or at an edge. In the latter case, two different loadings, namely tensile tractions applied on sides parallel to the major axis of the ellipsoid, and equal and opposite normal tractions applied on the vertical side coincident with the minor axis of the ellipsoid, are considered. In the former case, the body is loaded by tensile tractions applied on the far away surfaces that are parallel to the major axis of the ellipsoid. In each case, it is found that stresses and principal stretches at the void tip stay bounded, and the stress concentration factor depends upon the tractions applied at the far away surfaces.

1. INTRODUCTION

THE GROWING use of rubber components in critical parts such as shock absorbers and in vibration isolation bearings to separate dynamically loaded parts of the structure from the foundation necessitates a better understanding of the fracture mechanisms of these materials. The linear theory of elasticity—in conflict with its underlying approximations—predicts unbounded deformations and stresses near a crack tip. Most rubberlike materials can undergo large deformations in the elastic range. Knowles and Sternberg [1] have used the hodograph transformation method to study stresses near a crack tip in an elastic body made of a neo-Hookean material and deformed in antiplane shear. Subsequently, Fowler [2] used an asymptotic representation of the displacement field to study the same problem and obtained results in general agreement with those of Knowles and Sternberg [1]. These investigators found that for shearing in the z-direction, the component T_{zz} of the Cauchy stress tensor $\mathbf{T}$ becomes unbounded at the crack tip.

By analyzing the stress distribution in a plate made of a linear elastic material and containing an elliptical hole, Inglis [3] showed that the maximum stress at the major axis of the ellipse equalled $(1 + 2a/b)$ times the applied stress normal to the major axis at far away surfaces. Here $2a$ and $2b$ equal the major and minor axes of the ellipse. In this paper, we study the problem when a body made of Blatz–Ko material undergoes plane strain deformations, and consider two cases, namely when the body has an ellipsoidal void in its interior or it has a half elliptical void with its minor axis aligned along the left vertical surface. For the latter case, the body is loaded either by tensile tractions normal to the major axis of the ellipse and applied at far away surfaces, or equal and opposite normal tractions applied to the left vertical surface on either side of the void. The effect of varying the ratio of the major axis to the minor axis of the ellipse on the deformations of the body near the void tip is also examined.

2. FORMULATION OF THE PROBLEM

Since the deformed shape of the initially elliptical void is not known *a priori*, we use the referential or Lagrangian description of motion. In terms of rectangular Cartesian coordinates with the origin at the center of the undeformed void and the coordinate axes coinciding with its major and minor axes, equations governing the plane strain deformations of the body are

$$T_{i\alpha,\alpha} = 0, \quad i = 1, 2; \quad \alpha = 1, 2. \tag{1}$$

$\mathbf{T}$ is the first Piola–Kirchhoff stress tensor, a repeated index implies summation over the range of the index, and a comma followed by index α indicates partial differentiation with respect to X_α,

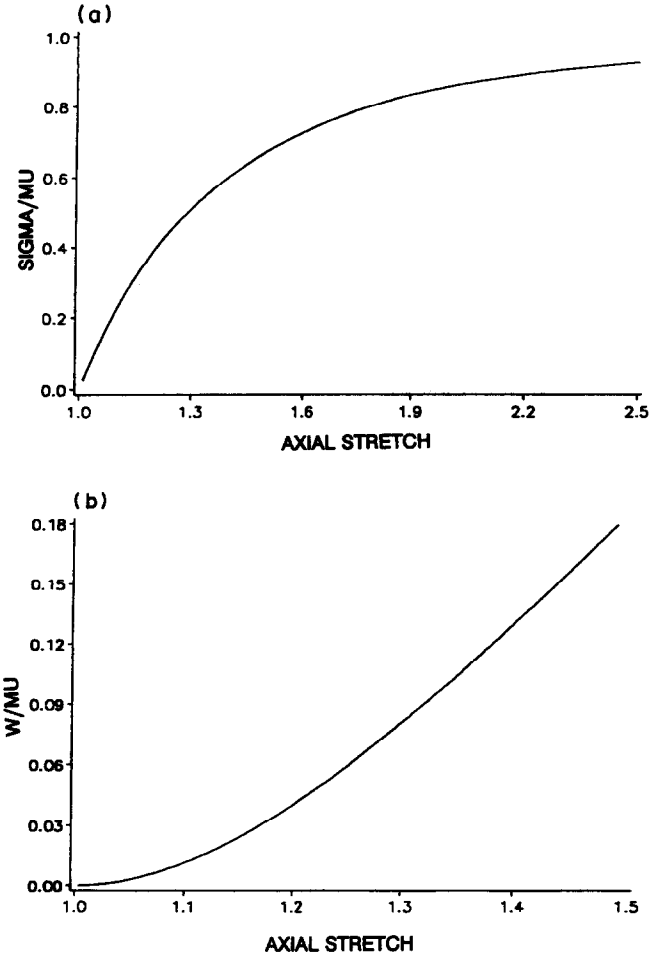

Fig. 1. Axial stress vs axial stretch, and strain energy density W per unit reference volume vs axial stretch for a Blatz–Ko material deformed in simple tension.

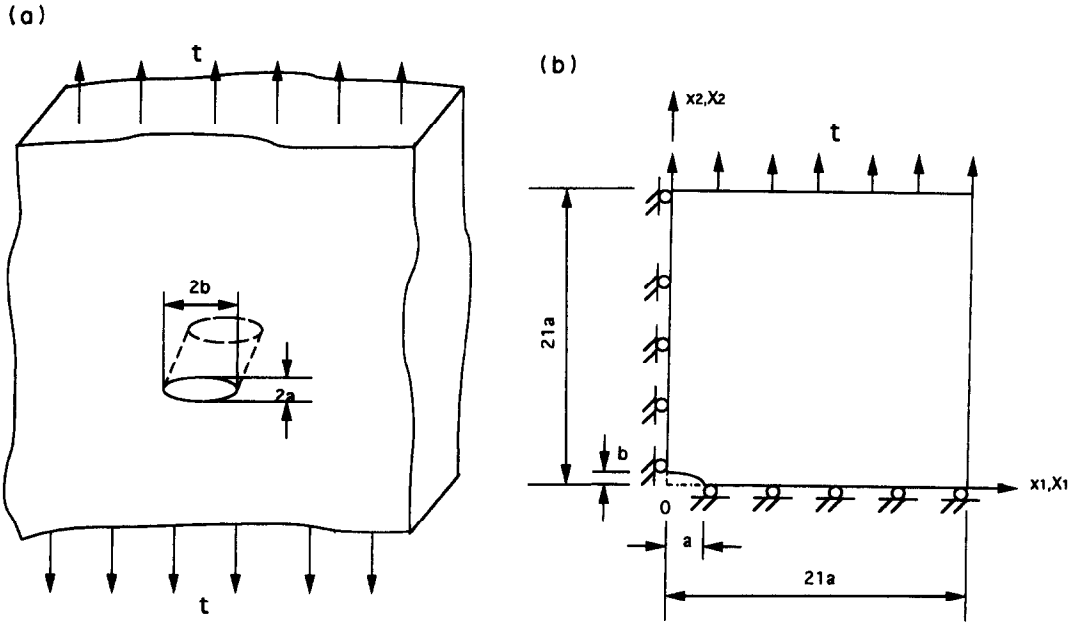

Fig. 2. Schematic sketch and the finite domain analyzed for problem 1.

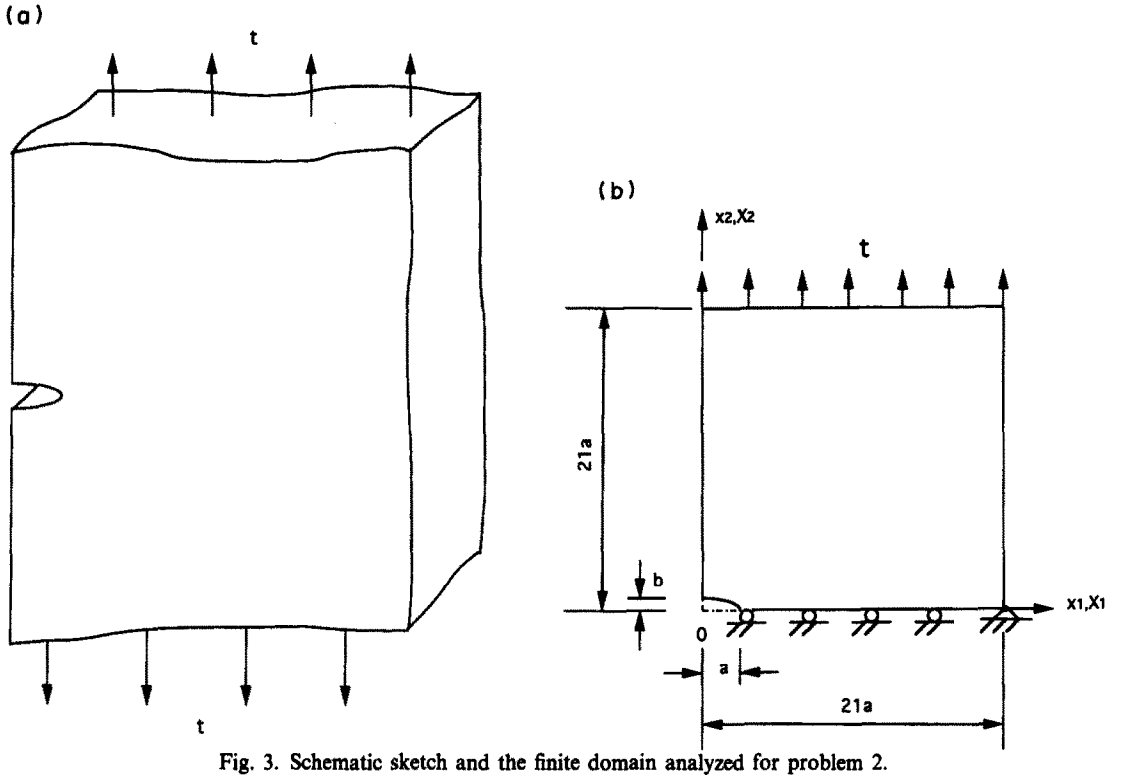

Fig. 3. Schematic sketch and the finite domain analyzed for problem 2.

which is the position of a point in the unstressed reference configuration. The Piola–Kirchhoff stress tensor is related to the strain energy density W per unit reference volume by

$$T_{i\alpha} = \frac{\partial W}{\partial F_{i\alpha}}, \quad F_{i\alpha} = x_{i,\alpha}. \tag{2}$$

Here $\mathbf{F}$ is the deformation gradient, and x_i the present position of the material particle that occupied place X_α in the reference configuration. We assume that the body is made of a Blatz–Ko material [4]. For plane strain deformations of the Blatz–Ko material

$$W = \frac{\mu}{2}\left[\frac{(I-1)}{J^2} + 2J - 4\right], \tag{3}$$

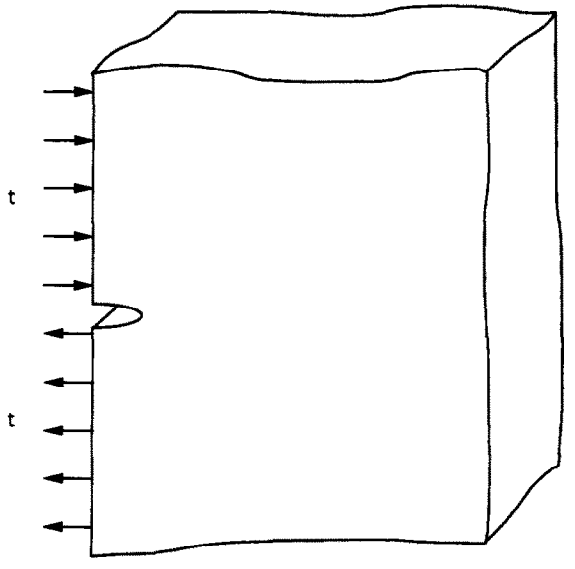

Fig. 4(a) (*caption overleaf*)

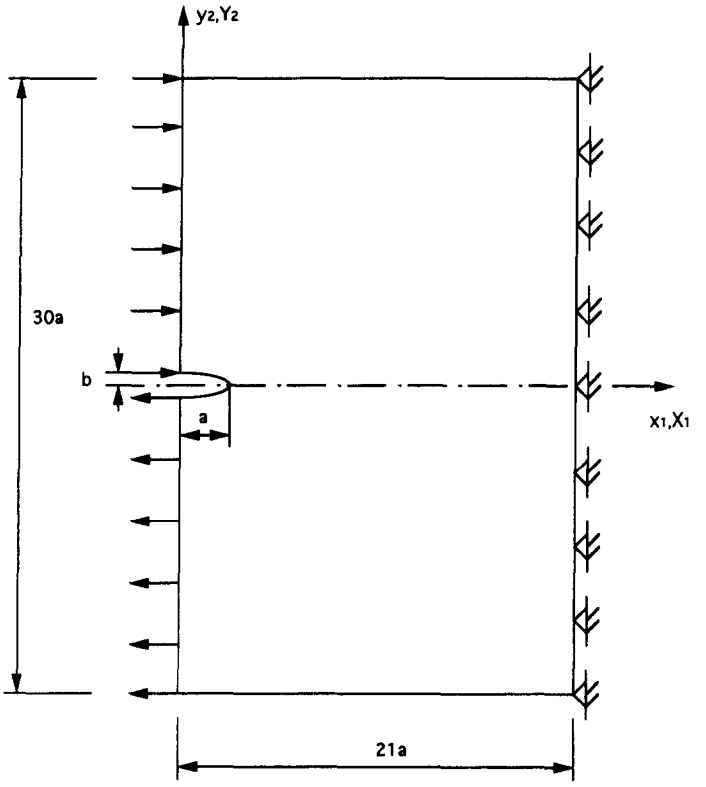

Fig. 4(b)
Fig. 4. Schematic sketch and the finite domain analyzed for problem 3.

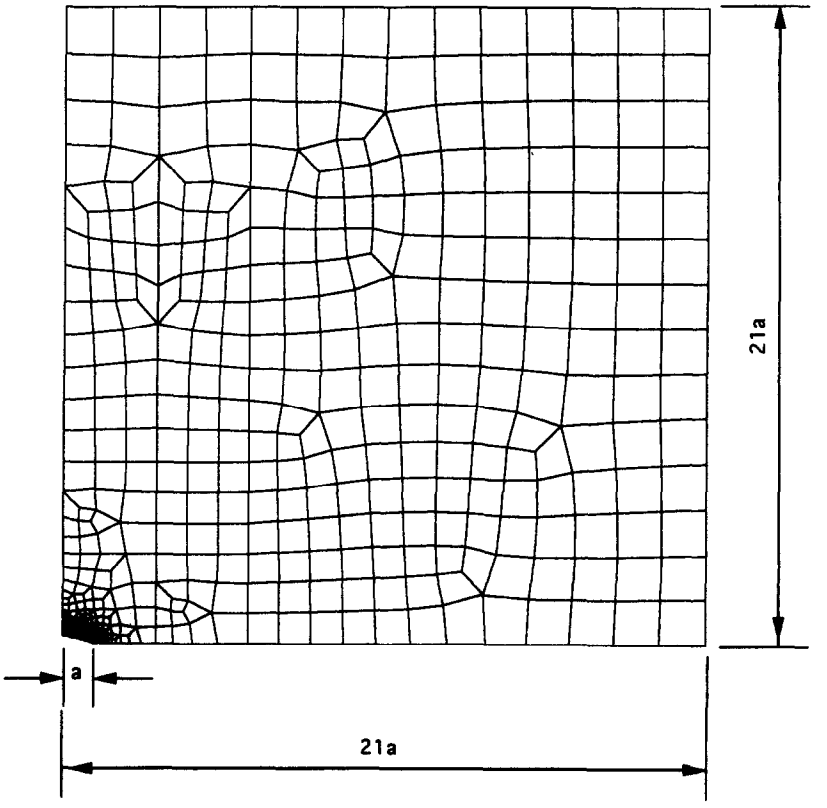

Fig. 5a. Finite element mesh, in the undeformed configuration, used to analyze the first problem for $a/b = 4$.

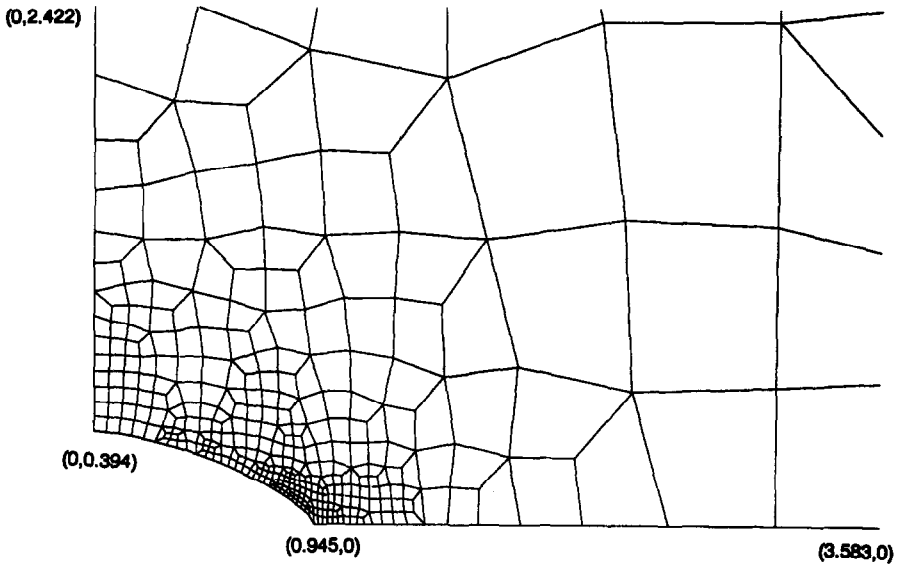

Fig. 5b. Deformed mesh in the vicinity of the void surface for $t/\mu = 0.15$.

where

$$J = \det \mathbf{F}, \quad I = \mathrm{tr}(\mathbf{F}\mathbf{F}^T) = \mathrm{tr}(\mathbf{F}^T\mathbf{F}). \tag{4}$$

In these equations, μ is the shear modulus of the material at zero strain. The Cauchy stress tensor $\boldsymbol{\sigma}$ is related to the first Piola–Kirchhoff stress tensor $\mathbf{T}$ by

$$\boldsymbol{\sigma} = J^{-1}\mathbf{T}\mathbf{F}^T. \tag{5}$$

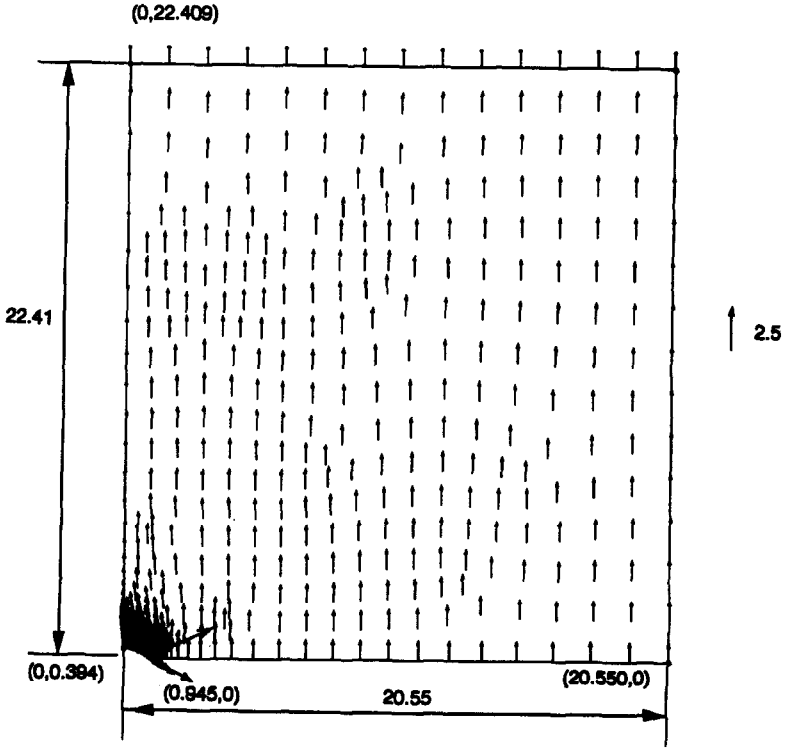

Fig. 6(a$_1$) (*caption overleaf*).

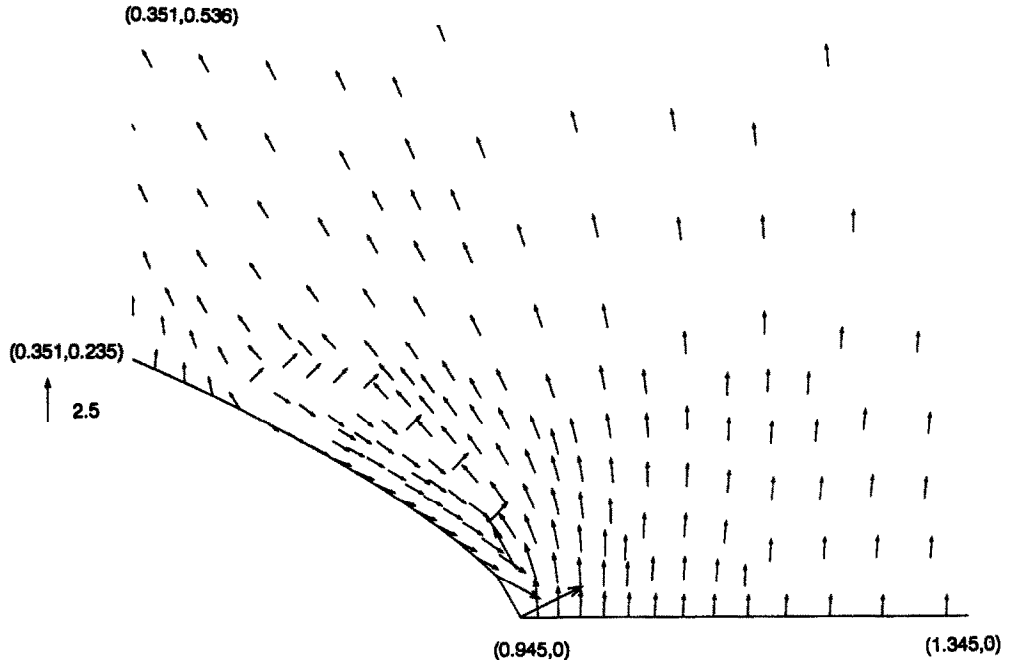

Fig. 6(a_2)

Fig. 6a. Variation of the maximum principal stretch within the domain for $t/\mu = 0.15$ and for the first problem.

Thus, for plane strain deformations of the Blatz–Ko material

$$\boldsymbol{\sigma} = \mu\left(1 - \frac{I}{J^3}\right)\mathbf{1} + \frac{\mu}{J^3}\mathbf{B}, \tag{6}$$

where

$$\mathbf{B} = \mathbf{F}\mathbf{F}^T \tag{7}$$

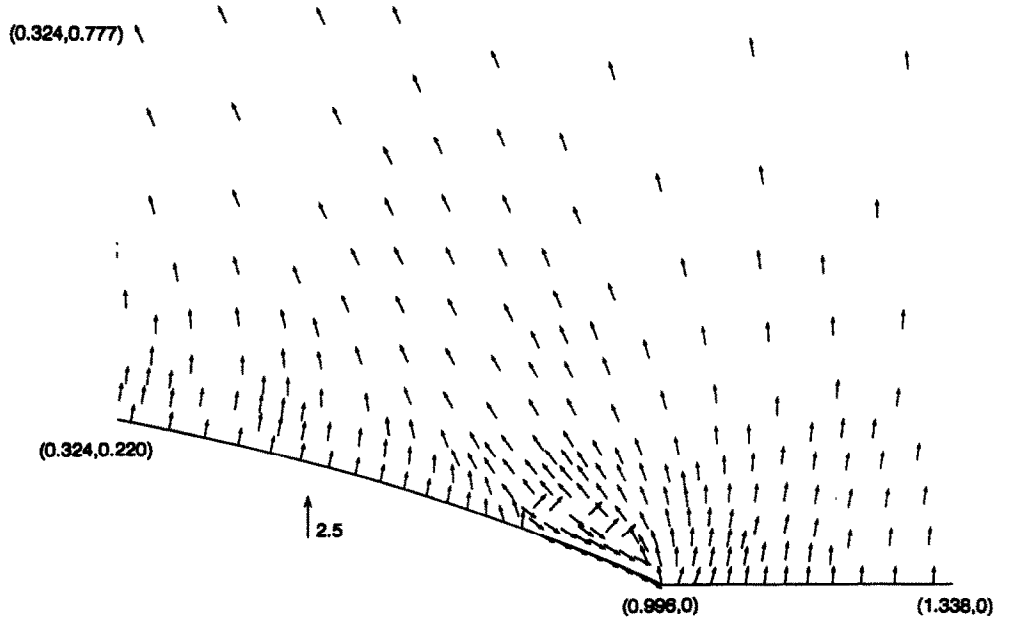

Fig. 6b. Variation of the maximum principal stretch in the vicinity of the crack surface for $t/\mu = 0.01$.

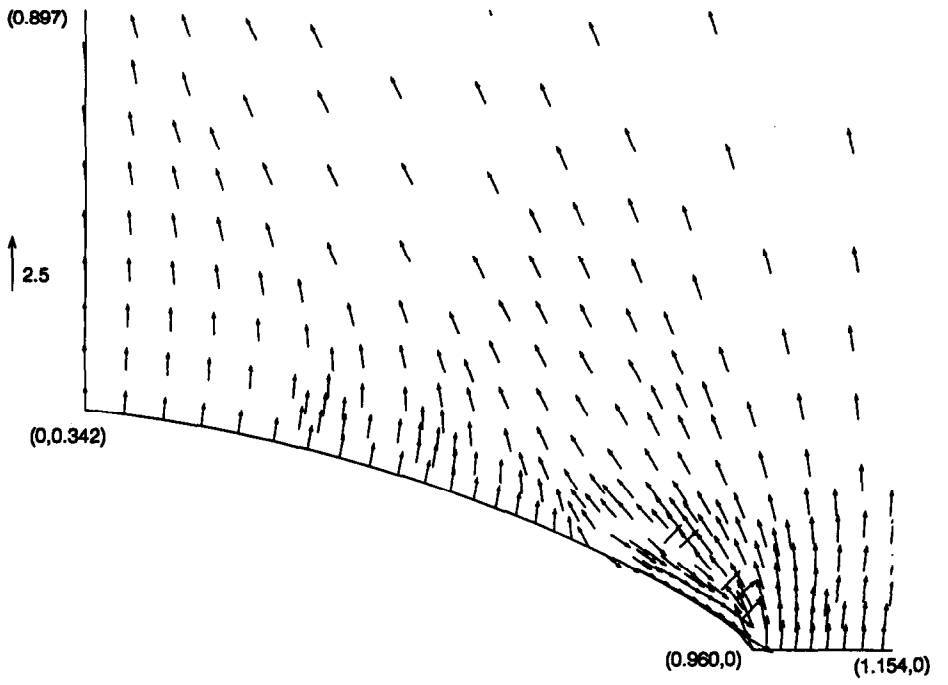

Fig. 6c. Variation of the maximum principal stretch in the vicinity of the crack surface for $t/\mu = 0.1$.

is the left Cauchy–Green tensor. The stress–strain curve and the strain energy density vs axial stretch curve for a Blatz–Ko material depicted in Fig. 1 indicate that the axial stress reaches a limiting value with an increase in the axial stretch, and the strain energy density continues to increase unboundedly for large axial stretches.

Substitution from eqs (2) through (7) into eq. (1) gives two coupled highly nonlinear partial differential equations which ought to be solved for x_1 and x_2 under the pertinent boundary conditions. Here we study the following three problems.

As the first problem, we study finite plane strain deformations of an infinite body containing an ellipsoidal cavity and subjected at infinity to tensile loads perpendicular to the major axis of the ellipsoidal void. Schematic sketches of the problem studied and of the finite domain analyzed are shown in Fig. 2. Here we have assumed that the deformations of the body are symmetrical about the horizontal and vertical centroidal axes and, thus, study deformations of the material in the first quadrant only. The horizontal and vertical dimensions of the region studied are chosen large enough so that their locations have a negligible effect on the deformations of the body in the vicinity of the void. The applicable boundary conditions are

$$\begin{aligned} T_{i2} &= t\delta_{i2} && \text{on the upper horizontal surface} \\ T_{i1} &= 0 && \text{on the right vertical surface} \\ x_1 = X_1, \quad T_{21} &= 0 && \text{on the left vertical surface} \\ T_{i\alpha}N_\alpha &= 0 && \text{on the void surface} \\ x_2 = X_2, \quad T_{12} &= 0 && \text{on the bottom horizontal surface.} \end{aligned} \tag{8}$$

The boundary conditions due to the assumed symmetry of deformations hold on the left and bottom surface, the right surface is taken to be traction free, and uniform tensile tractions are applied on the top surface.

In the second problem, the body has a half ellipsoidal void with its minor axis coincident with the left vertical surface and tensile loads perpendicular to the major axis of the ellipsoid are applied to the top and bottom surfaces. The deformations of the body are taken to be symmetrical about

the horizontal centroidal axis. Accordingly, we study deformations of the upper half of the body. Schematic sketches of the problem studied and of the finite domain analyzed are shown in Fig. 3. The pertinent boundary conditions are

$$T_{i2} = t\delta_{i2} \quad \text{on the upper horizontal surface}$$

$$T_{i1} = 0 \quad \text{on the left vertical surface}$$

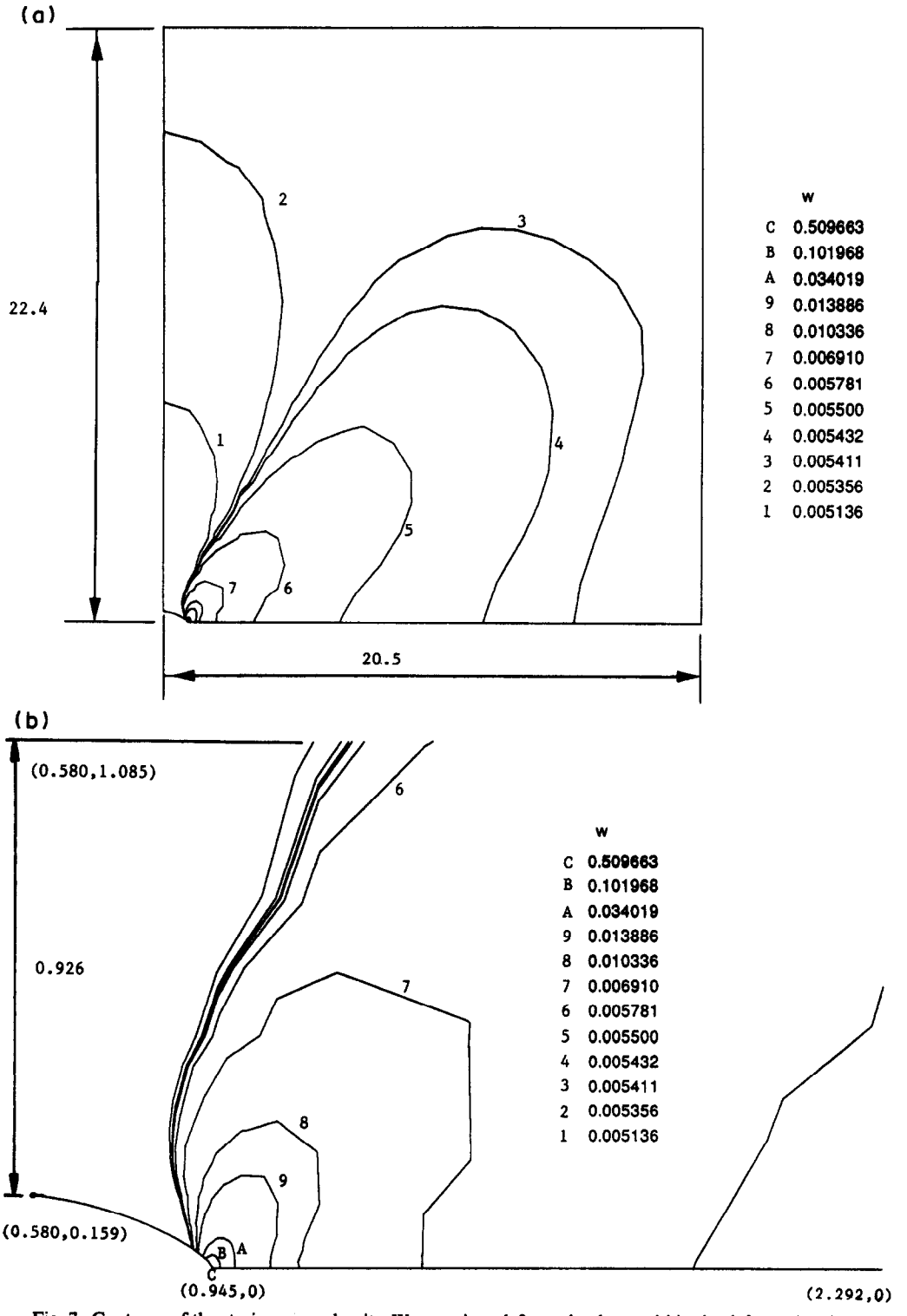

Fig. 7. Contours of the strain energy density W per unit undeformed volume within the deformed region.

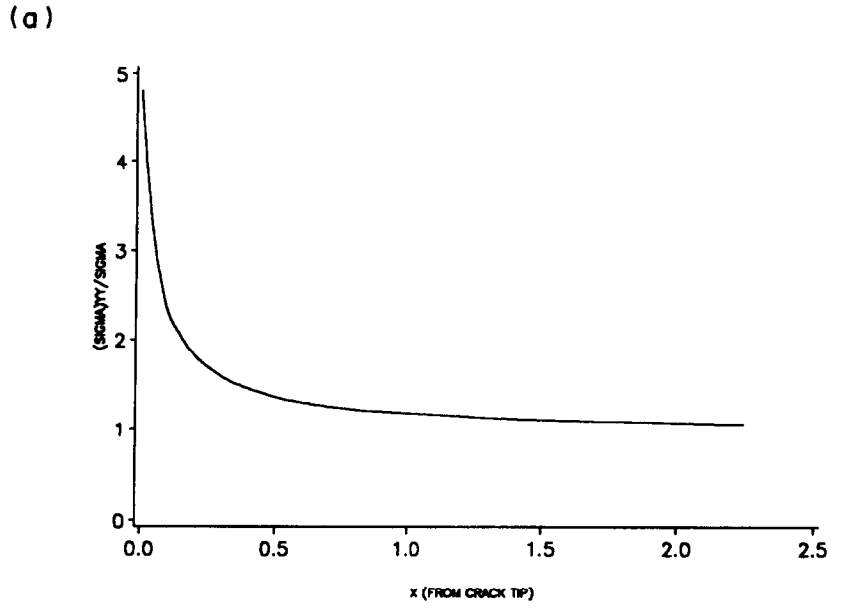

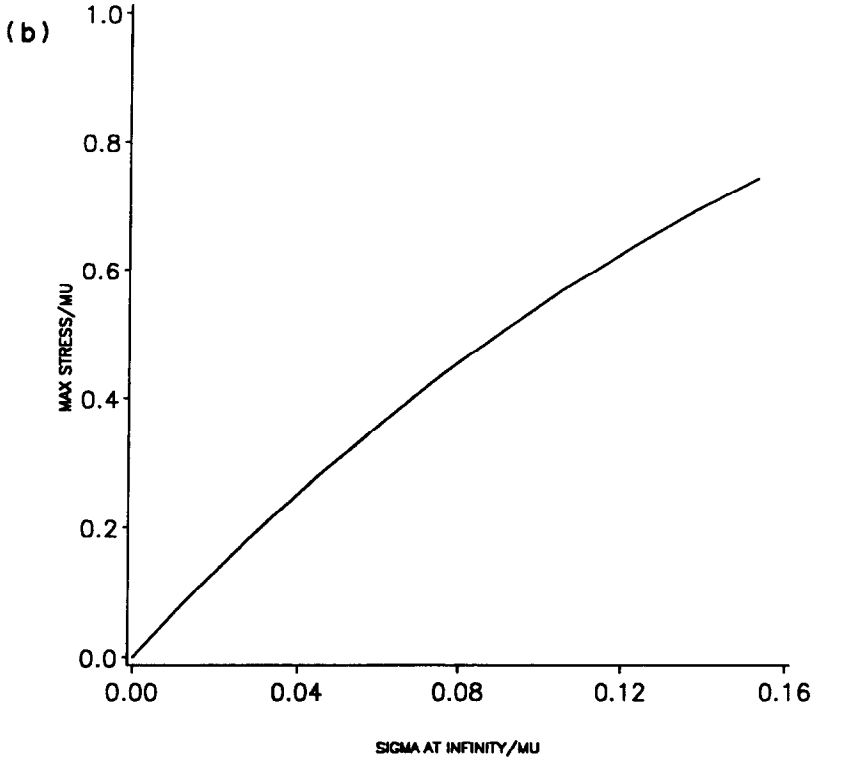

Fig. 8a. The ratio σ_{yy}/σ vs distance from the crack tip at points on the horizontal axis through the crack tip for $t/\mu = 0.15$.

Fig. 8b. Maximum stress at the crack tip vs the applied traction.

$$\begin{aligned} T_{i1} &= 0 && \text{on the right vertical surface} \\ T_{i\alpha} N_\alpha &= 0 && \text{on the void surface} \\ x_2 = X_2, \quad T_{12} &= 0 && \text{on the bottom horizontal surface;} \end{aligned} \tag{9}$$

and the bottom right corner is kept fixed to eliminate the rigid body motion.

For the third problem, we assume that the body has a half ellipsoidal void with its minor axis abutting the left vertical surface of the body. Equal and opposite normal loads are applied on this

surface with the remaining surfaces held traction free. The finite domain analyzed is shown in Fig. 4 with the following boundary conditions applied on its surfaces.

$$\begin{aligned} T_{i2} &= 0 && \text{on the upper and bottom horizontal surfaces} \\ x_i &= X_i && \text{on the right vertical surface} \\ T_{i1} &= -t\delta_{i1} && \text{on the left vertical surface above the void} \\ T_{i1} &= t\delta_{i1} && \text{on the left vertical surface below the void} \\ T_{i\alpha}N_\alpha &= 0 && \text{on the void surface.} \end{aligned} \tag{10}$$

Each of the three problems formulated above is difficult to solve analytically, so we seek approximate solution by the finite element method.

3. NUMERICAL SOLUTION AND RESULTS

In order to solve any one of these problems numerically, we use the Galerkin approximation [5] to obtain its weak formulation that incorporates natural boundary conditions. The finite region studied is divided into four-noded quadrilateral subdomains. The displacement field is approximated by a bilinear function on each quadrilateral so that over the entire domain it is represented by a piecewise linear continuous function. Substitution of this displacement field into the weak formulation of the problem gives a set of nonlinear algebraic equations which are solved iteratively by the Newton–Raphson method. The applied load is divided into several steps, and within each load step, equilibrium iterations are performed until, at each node point

$$\frac{|\Delta \mathbf{u}|}{|\mathbf{u}|} \leqslant 10^{-3}, \tag{11}$$

where $\Delta\mathbf{u}$ is the just-computed increment in the nodal displacement because of the unbalanced forces and $\mathbf{u}$ is the total computed displacement of that node. We used the 2×2 Gauss quadrature rule to evaluate various integrals numerically.

The developed code was validated by analyzing the simple tension problem, the simple shearing problem, and the plane strain problem of an infinite elastic body made of a Blatz–Ko material and containing a circular cavity. The last problem with a uniform pressure applied to the

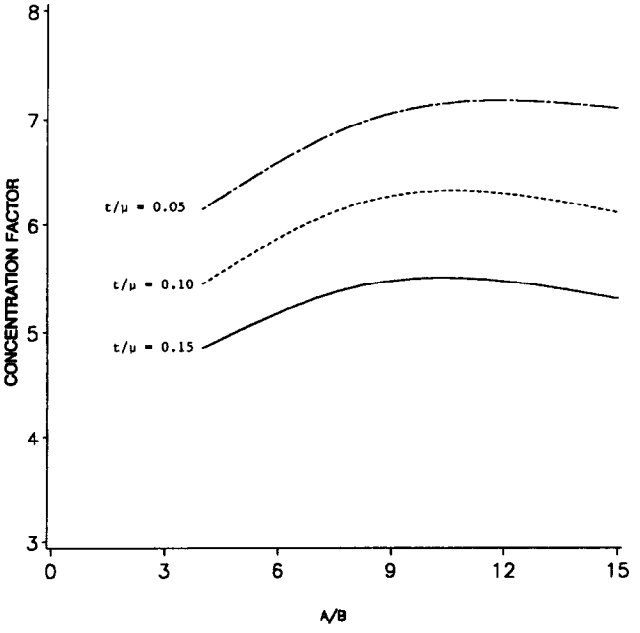

Fig. 9. The stress concentration factor vs a/b for problem 1 and for $t/\mu = 0.05$, 0.10, and 0.15.

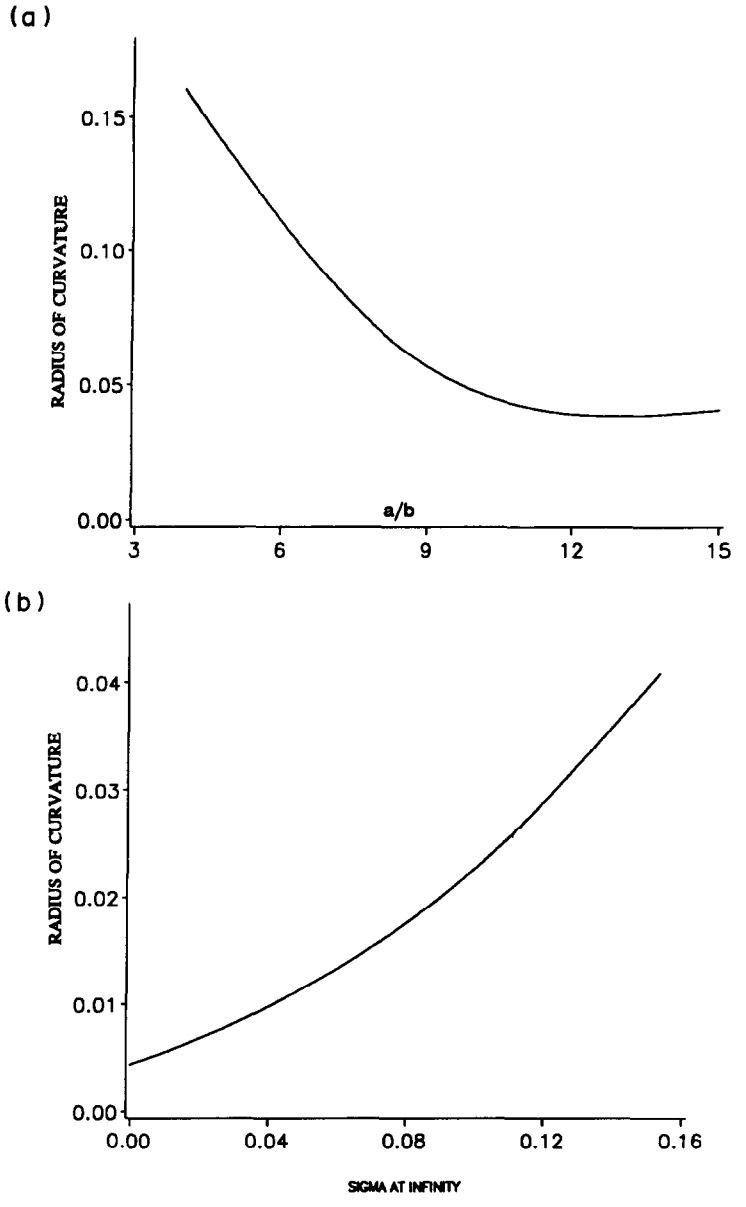

Fig. 10a. Radius of curvature of the deformed crack tip vs a/b.

Fig. 10b. Radius of curvature of the deformed crack tip vs the normal traction applied at the far away surface.

void surface has been studied analytically by Abeyaratne and Horgan [6]. The maximum difference between the values of the hoop stress at any point on the inner surface of the void as obtained from the analytical solution and the numerical solution was found to be less than 1%.

3.1. *Results for the first problem*

Figure 5a depicts the finite element mesh, in the undeformed configuration with $a/b = 4$ for the ellipsoidal void, that is used to analyze the first problem; a blow-up of the mesh around the ellipsoidal void in the deformed configuration is shown in Fig. 5b. In this and subsequent figures, the length scale has been normalized with respect to the semi-major axis of the ellipsoidal void in the undeformed configuration. The mesh used is very fine in the vicinity of the crack tip and gradually becomes coarser as one moves away from it. Figure 5b reveals that the crack tip has been blunted during the deformation. That the deformation of the body is homogeneous everywhere except in the vicinity of the crack should be apparent from the plot of the maximum principal

stretch given in Fig. 6a for $t/\mu = 0.15$. It establishes that the domain considered is adequate. Recalling that the length of the vector is proportional to the magnitude of the maximum principal stretch and it occurs along the vector shown, the deformation is extremely complex near the crack tip. The peak value of the maximum principal stretch occurs at the crack tip and is finite as compared to the infinite value predicted by the linear theory of elasticity. Note that the width of

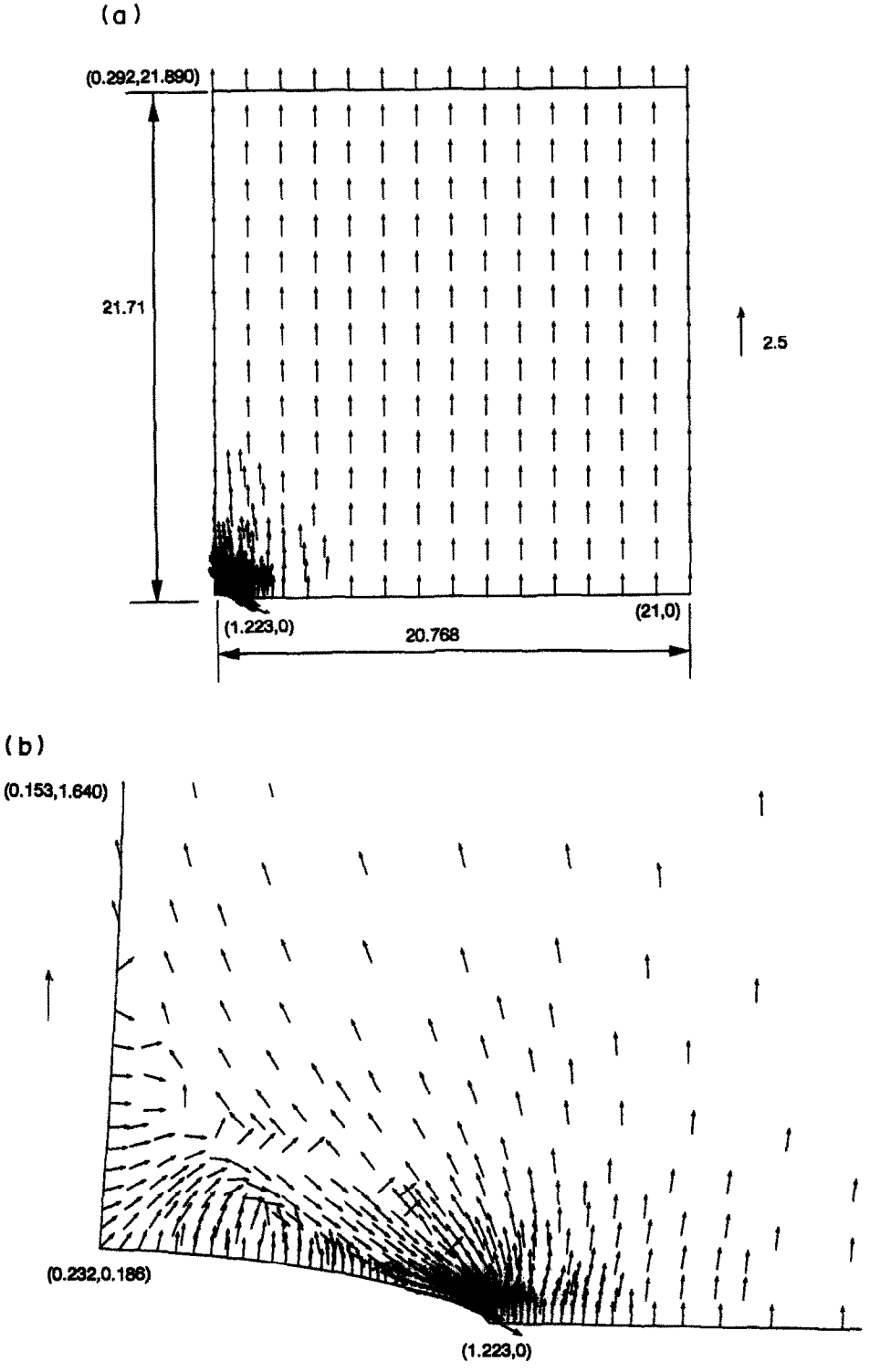

Fig. 11. Distribution of the maximum principal stretch within the deformed domain for $a/b = 15$ and $t/\mu = 0.1$ for problem 2.

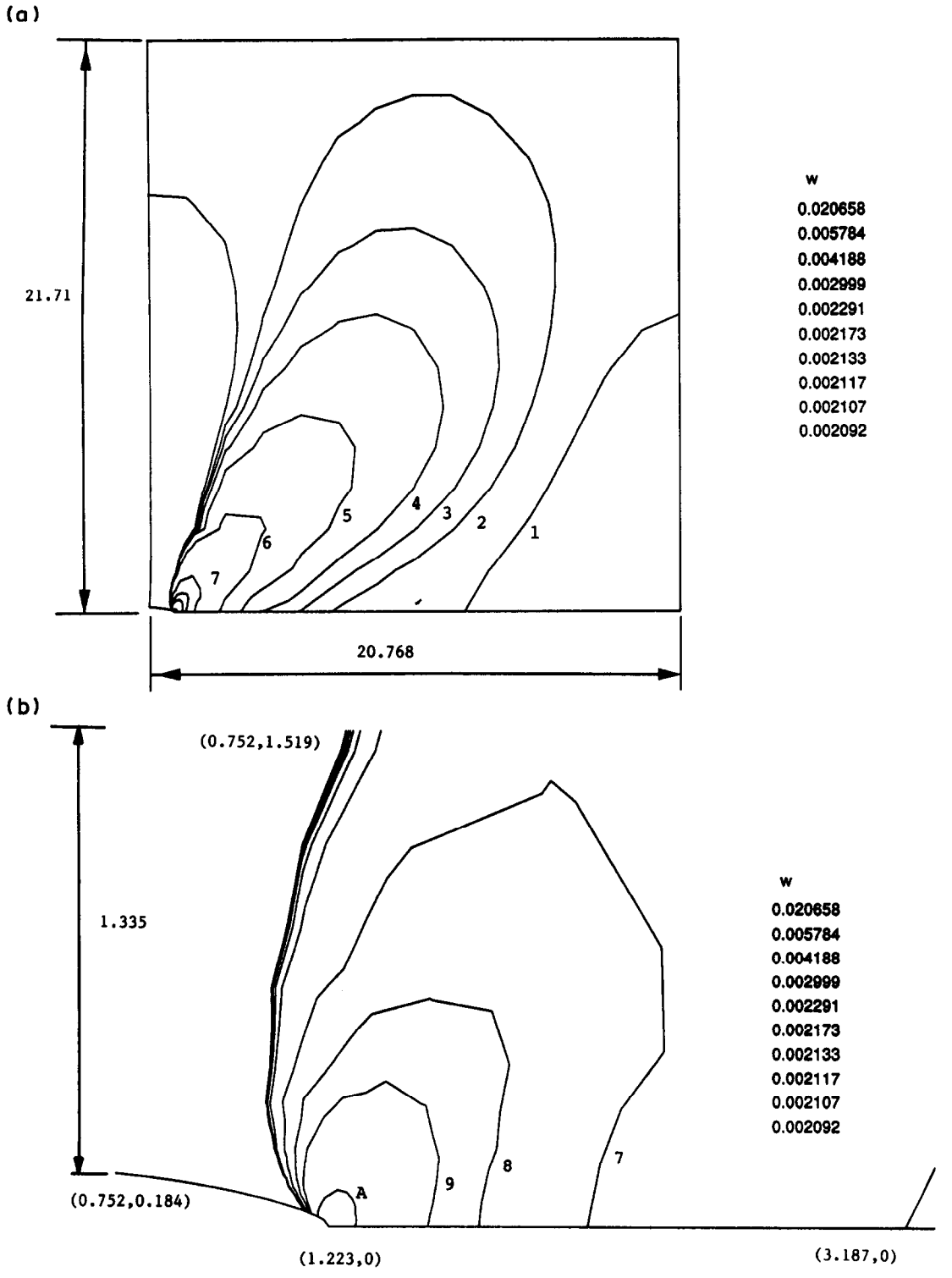

Fig. 12. Contours of the strain energy density W per unit undeformed volume for problem 2.

the region studied has contracted significantly because of the tensile tractions applied on the top horizontal surface. The plots of the maximum principal stretch in the deformed region around the crack surface for $t/\mu = 0.01$ and 0.1 are given in Figs 6b and 6c, respectively. Their comparison with the plot of Fig. 6a indicates that the deformation of the crack tip depends noticeably upon

the applied traction, and the direction and magnitude of the maximum principal stretch at the crack tip depend in a complicated way upon the applied surface tractions on the top horizontal surface.

The contours in the present configuration of the strain energy density W per unit undeformed volume are depicted in Fig. 7 for $t/\mu = 0.15$. That the strain energy density stays finite at points near the crack tip confirms the assertion made above that the deformations at points near the crack tip stay bounded. It is clear that W decays fairly rapidly as one moves away from the crack tip. The values of σ_{yy}/σ at points on the horizontal axis through the crack tip are plotted in Fig. 8a. The abscissa equals the distance from the crack tip, and σ is the tensile traction measured per unit deformed area applied on the top horizontal surface, whereas t is measured per unit undeformed area. According to the linear theory of elasticity, σ_{yy}/σ at the crack tip should equal 9 for $a/b = 4$.

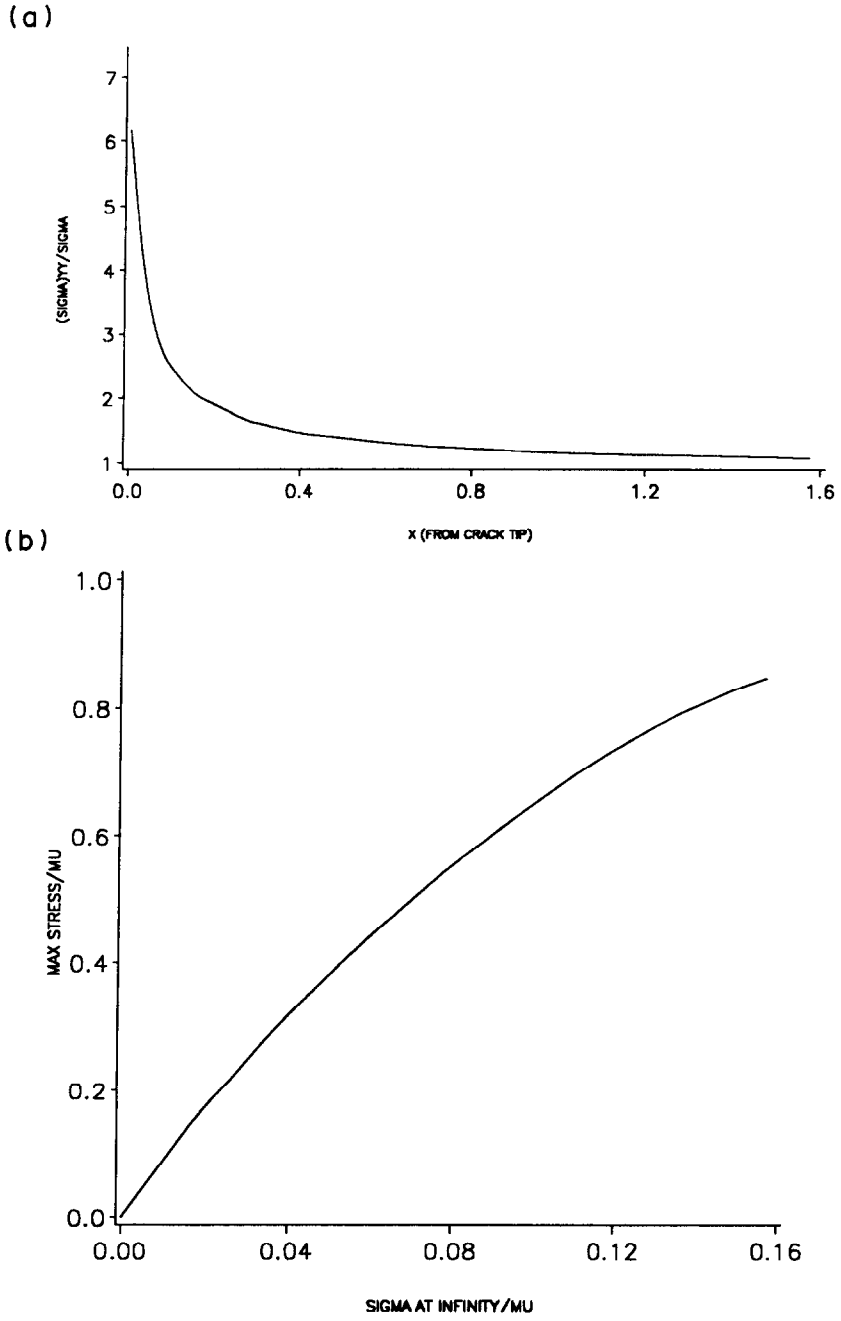

Fig. 13a. Distribution of the normal stress σ_{yy}/σ at points on the horizontal axis through the void tip.

Fig. 13b. The normal stress σ_{yy} at the void tip vs the applied normal traction σ at the far away surface.

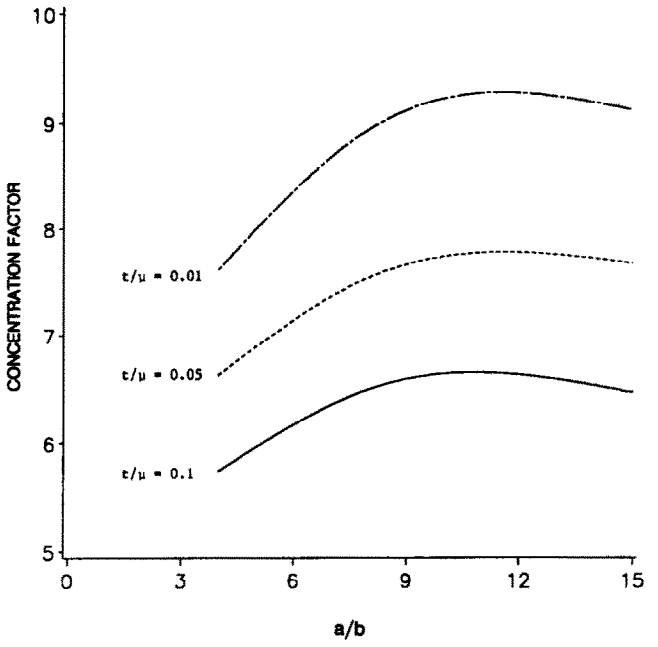

Fig. 14. Dependence of the stress concentration factor K upon the ratio a/b.

For the nonlinear problem being discussed, we obtain 5.6 for σ_{yy}/σ at the crack tip. However, the slope at $\sigma = 0$ of the curve depicting σ_{yy} at the crack tip vs σ in Fig. 8b is found to be 7.54. The dependence of the stress concentration factor K, defined as σ_{yy} at the crack tip/σ at the top surface, upon the ratio a/b is shown in Fig. 9. Whereas the linear theory of elasticity predicts this curve to be a straight line of slope 2, irrespective of the load applied, we obtain a nonlinear dependence of the stress concentration factor upon a/b, and its values depend upon the applied traction at far away surfaces. For each value of the applied traction K first increases with an increase in the value of a/b and plateaus out for large values of a/b. The asymptotic value of K is higher for lower values of the applied traction.

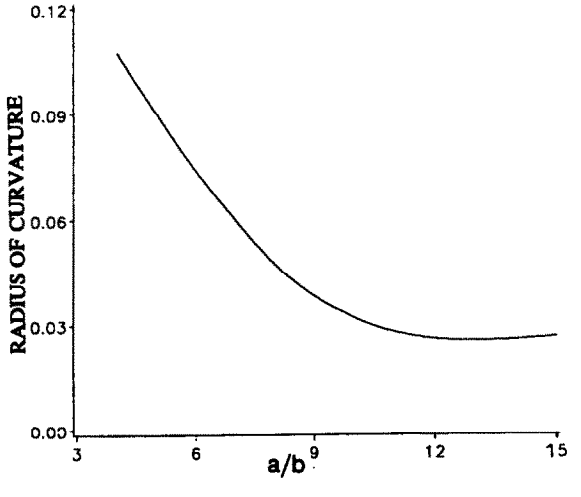

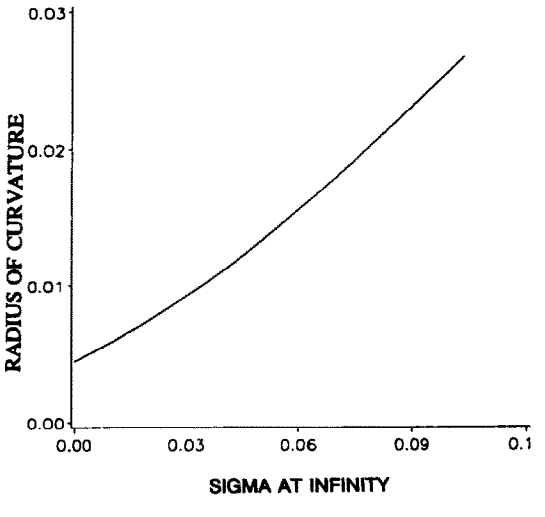

Fig. 15a. Radius of curvature of the deformed void tip vs a/b.

Fig. 15b. Radius of curvature of the deformed void tip vs the normal traction applied at the far away surface.

The dependence of the radius of curvature of the deformed crack tip upon the ratio a/b and upon the normal traction applied at the far away surface is shown in Figs 10a and 10b, respectively. For applied traction $t = 0.15\mu$, the radius of curvature of the deformed void tip decreases with an increase in the value of a/b until it reaches the minimum value of 0.04 for $a/b = 12$, and then it increases very slowly. For $a/b = 4$, the radius of curvature of the deformed void tip continues to increase with an increase in the value of the tensile traction applied at the far away surfaces.

3.2. *Results for the second problem*

Figure 11 exhibits the distribution and direction of the maximum principal stretch at various points within the deformed domain for $a/b = 15$ and $t/\mu = 0.1$. It is clear that the deformation of the body at points near the void surface, and especially of points close to the void tip, is extremely complicated. As for the first problem, the vector of the maximum principal stretch is normal to the void surface at most of the points except near its boundaries. At points near the void tip, the maximum principal stretch is directed along the deformed void surface. Because of severe deformations near the void tip, the radius of curvature there changes appreciably. The contours

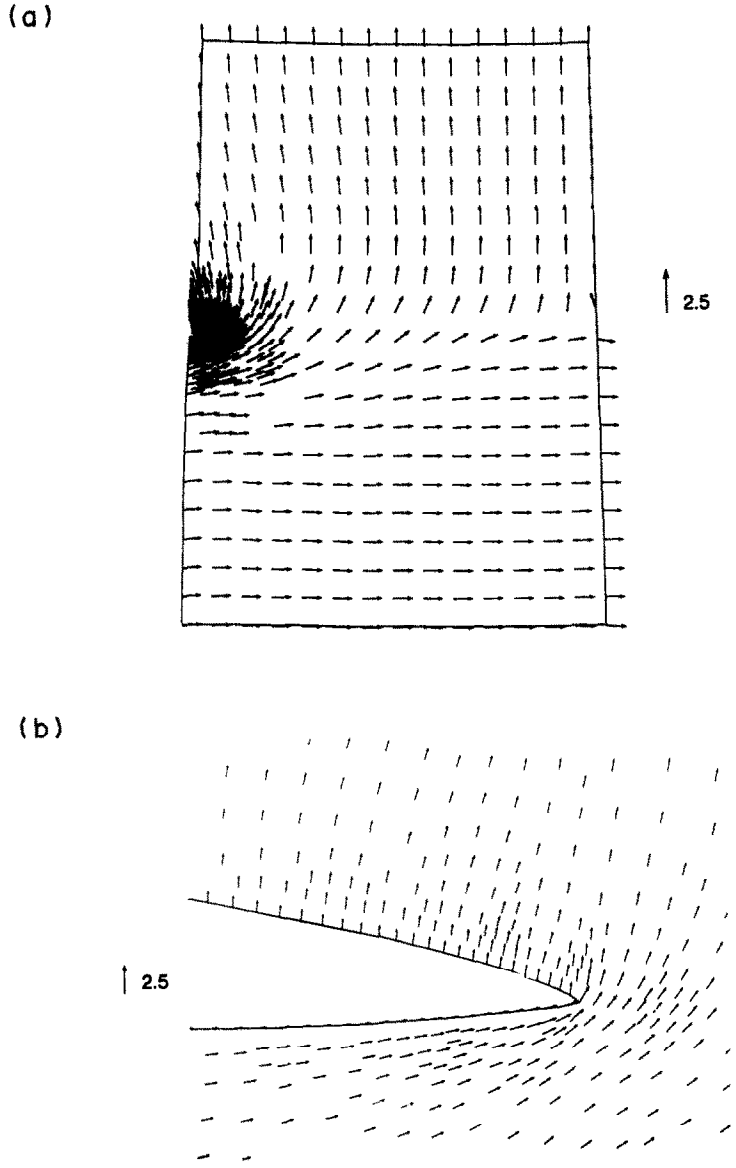

Fig. 16. Distribution of the maximum principal stretch within the deformed region for $a/b = 15$ and $t/\mu = 0.1$ for the third problem.

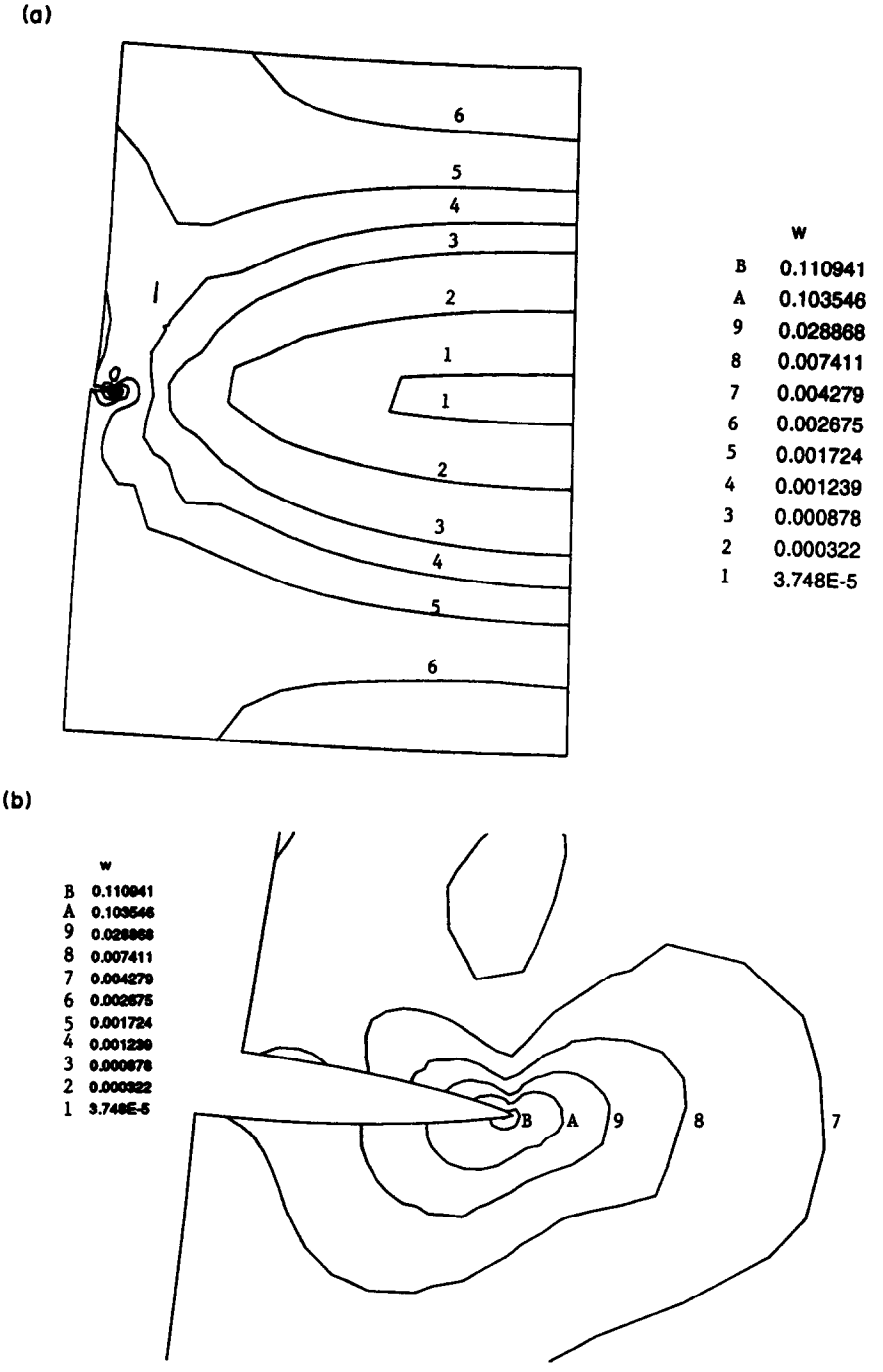

Fig. 17. Contours of the strain energy density W per unit undeformed volume for problem 3.

in the present configuration of the strain energy density W per unit undeformed volume are plotted in Fig. 12. The peak value of W occurs at the void tip and it decays quite rapidly with the distance from the void tip. Note that beyond the fifth contour around the void tip, W changes from 0.002173 to 0.002092, implying thereby that the deformation of the region outside of the fifth contour is essentially homogeneous. In Fig. 13, we have plotted the variation of σ_{yy} at points on the horizontal axis through the void tip, and σ_{yy} at the void tip vs the applied traction σ at the far away surface. The stress σ_{yy} decays very rapidly with the distance from the void tip. For a linear elastic material, σ_{yy} at the void tip is proportional to the applied traction σ. For the nonlinear material being studied here, the dependence of σ_{yy} at the void tip upon σ is nonlinear and the ratio of the two, often called the stress concentration factor K, depends upon σ. Since σ_{yy} reaches a plateau at large values of

σ, the stress concentration factor first increases and then decreases with an increase in the value of σ.

Figure 14 shows the dependence of the stress concentration factor K upon the ratio a/b for $t/\mu = 0.01$, 0.05, and 0.1. In each case, K first increases with an increase in the value of a/b and then appears to reach a limiting value; the limiting value depends upon the applied traction and is highest for $t/\mu = 0.01$. In Figs 15a and 15b, we have plotted the radius of curvature of the deformed void tip vs the ratio a/b for a fixed value of the applied traction, and for $a/b = 15$, the dependence of the radius of curvature of the deformed void tip upon the tensile traction applied at the far away surfaces. These curves are similar to those for the first problem.

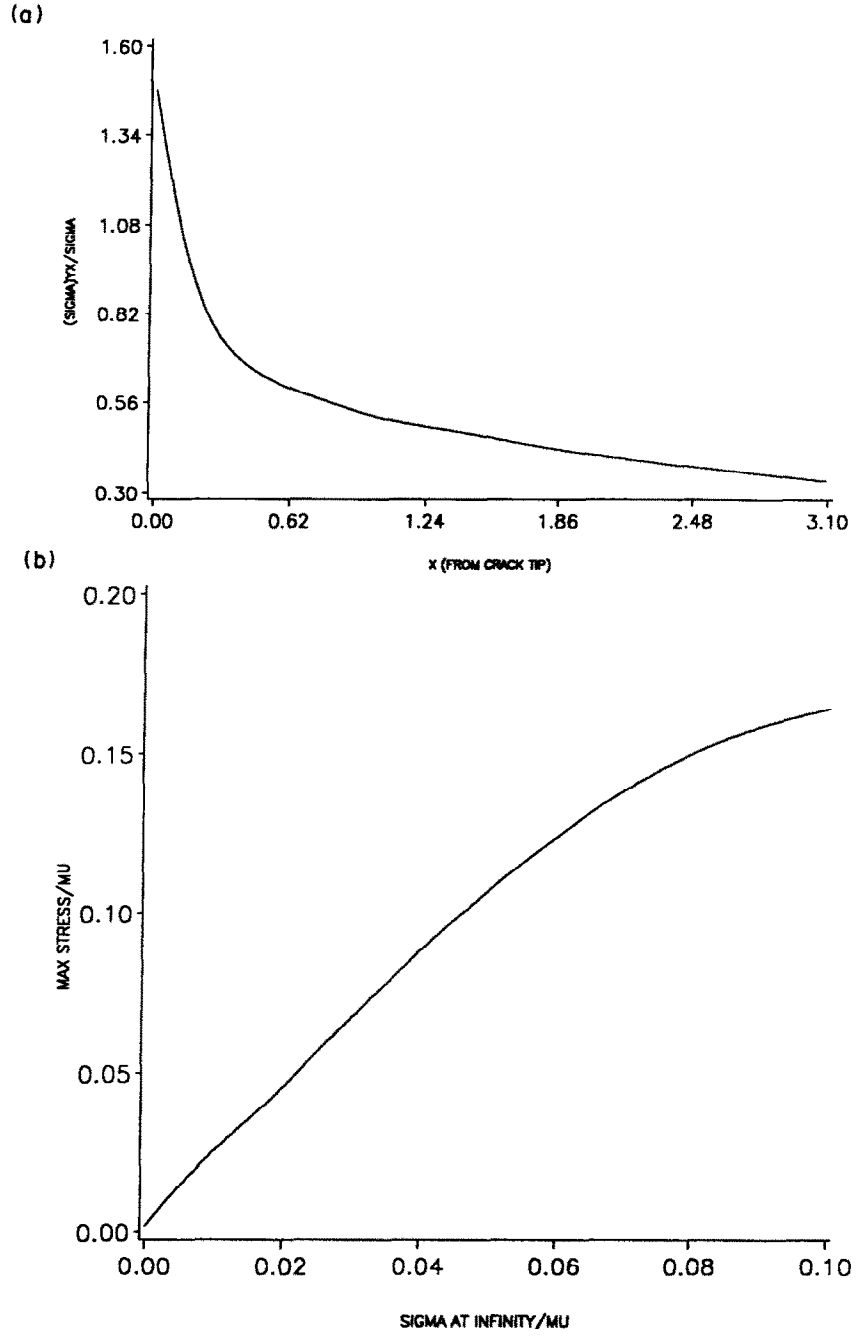

Fig. 18a. Distribution of the shear stress σ_{12} at points on the horizontal axis through the void tip.

Fig. 18b. Dependence of the maximum shear stress σ_{12} upon the tractions applied on the left face.

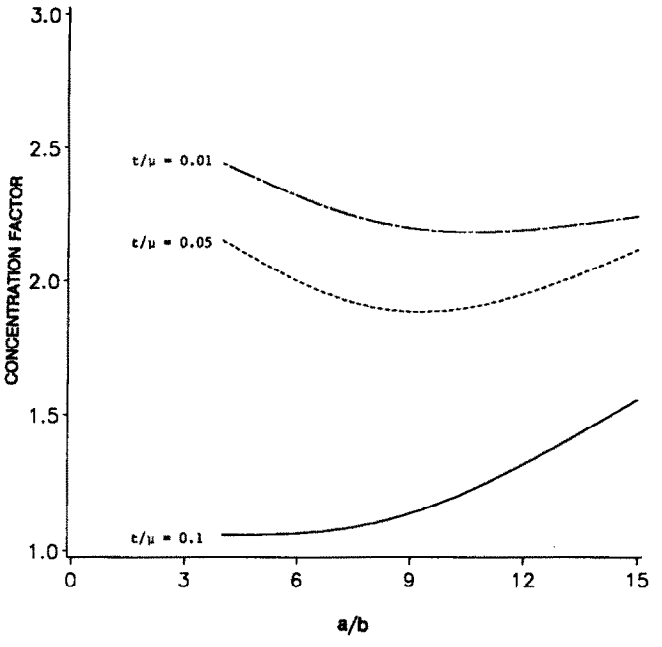

Fig. 19. Dependence of the stress concentration factor upon the ratio a/b.

3.3. *Results for the third problem*

In this problem, the part of the left vertical surface above the void is subjected to normal compressive tractions and that below the void to equal normal tensile tractions; the right vertical surface is held stationary. Figure 16 depicts the distribution of the maximum principal stretch at various points in the deformed region, and also in the vicinity of the void surface for $t/\mu = 0.1$ and $a/b = 15$. It is reasonable to expect that the applied loads will induce tensile deformations in the horizontal direction in the region below the horizontal line through the void tip and compressive deformations in the region above this line. Since we have plotted the maximum principal stretch, the directed lines in the lower half of the body are parallel to the applied tensile load, and those in the upper half of the body are perpendicular to the applied compressive load. The void tip is not deformed as much as it is in the second problem, and the maximum principal stretch at the void tip is not as large as it is in the previous two cases. The maximum principal stretch on the lower surface of the void is along the surface, that on the upper surface of the void is nearly vertical.

The contours in the present configuration of the strain energy density W per unit undeformed volume plotted in Fig. 17 indicate that material points on the upper surface of the void that are near the void tip are deformed more severely as compared to those on the lower surface of the void. The strain energy density decays rapidly with the distance from the void tip, signifying that much of the region away from the void surface has been deformed homogeneously. Figure 18a depicts the variation of the shear stress σ_{12} at points on the horizontal line through the void tip. As one moves away from the void tip, the shear stress drops very rapidly initially and then quite slowly. The rate of drop of the shear stress with the distance from the void tip is much less as compared to that of the normal stress at similarly situated points in the previous two problems. The variation of the maximum shear stress σ_{12} at the void tip upon the normal traction σ applied on the left vertical surface, plotted in Fig. 18b, indicates that σ_{12} equals nearly 2σ; the dependence of σ_{12} upon σ is, of course, nonlinear. However, the nonlinear effects manifest themselves for higher values of σ.

The dependence of the stress concentration factor K, defined as σ_{12} at the void tip divided by the normal traction σ on the left vertical surface, upon the ratio a/b, shown in Fig. 19, indicates that for $t = 0.01\mu$, K first decreases with an increase in the value of a/b and eventually reaches a plateau. However, for $t = 0.05\mu$, K decreases when a/b is increased from 4, takes on a minimum value for $a/b = 9$, and then increases with an increase in the value of a/b. For a higher value of the applied traction, namely, $t = 0.1\mu$, K first increases very slowly when a/b is increased from 4

to 6, but quite rapidly for higher values of a/b. The dependence of K upon a/b in this case is quite different from that in the previous two cases wherein K attained a limiting value when a/b was increased.

4. CONCLUSIONS

We have studied plane strain deformations of a body made of a Blatz–Ko elastic material and containing an ellipsoidal void. Three different problems, sketched in Figs 2, 3 and 4, are studied by the finite element method. In each case, the applied loads induce finite deformations of the body, and the void tip is deformed severely. The deformations of the material close to the void surfaces are too complicated to be described analytically. The peak value of the maximum principal stretch and of the strain energy density per unit volume in the reference configuration occurs at the void tip. The strain energy density decreases rapidly with the distance from the void tip. For each one of the three problems studied, the deformations of the material at the void tip stay bounded. The radius of curvature of the deformed void tip depends strongly upon the ratio a/b and also on the applied tractions.

Acknowledgements—This work was supported by the U.S. Army Research Office grant DAAL03-91-G-0084 to the University of Missouri-Rolla, and the University of Missouri Weldon Spring Fund.

REFERENCES

[1] J. K. Knowles and E. Sternberg, Discontinuous deformation gradients near the tip of a crack in finite anti-plane shear: an example. *J. Elasticity* **10**, 81–110 (1980).
[2] G. F. Fowler, Finite plane and anti-plane elastostatic fields with discontinuous deformation gradients near the tip of a crack. *J. Elasticity* **14**, 287–328 (1984).
[3] C. E. Inglis, Stresses in a plate due to the presence of cracks and sharp corners. *Trans. Inst. Nav. Arch.* **55**, 219–241 (1913).
[4] P. J. Blatz and W. L. Ko, Application of finite elasticity to the deformation of rubbery material. *Trans. Soc. Rheology* **6**, 223–251 (1962).
[5] T. J. R. Hughes, *The Finite Element Method. Linear Static and Dynamic Problems*. Prentice-Hall, Englewood Cliffs, NJ (1987).
[6] R. Abeyaratne and C. O. Horgan, Initiation of localized plane deformations at circular cavity in an infinite compressible nonlinearly elastic medium. *J. Elasticity* **15**, 243–256 (1985).

(*Received* 9 *September* 1992)